SST Sensitivities in Multiday TOGA COARE Cloud-Resolving Simulations

ALEXANDRE A. COSTA, WILLIAM R. COTTON, ROBERT L. WALKO, ROGER A. PIELKE SR., AND HONGLI JIANG

Department of Atmospheric Science, Colorado State University, Fort Collins, Colorado

(Manuscript received 5 May 1999, in final form 1 June 2000)

ABSTRACT

A two-dimensional cloud-resolving model (CRM) was used to simulate the evolution of convection over the western Pacific between 19 and 26 December 1992, during the Tropical Ocean Global Atmosphere Coupled Ocean–Atmosphere Response Experiment. A control simulation (CONTROL) was performed in which observed, time-evolving, spatially homogeneous SSTs were used as a lower boundary condition. It showed that the CRM was able to properly represent the evolution of the cloud systems.

Sensitivity experiments were carried out, in which the sea surface temperature was increased (SST+) or decreased (SST−) by 1°C and the same evolving large-scale forcing used in CONTROL. The similarities among all simulations suggested that the large-scale forcing is the dominant mechanism controlling the statistics of the cloud systems, including the total precipitation. However, the convective–stratiform partition of the cloud systems was altered, the convective part being favored in SST+ and the stratiform part favored in SST−. In terms of the radiative budget, the reduced low-level cloud coverage in SST+ acted to compensate the enhancement of high-cloud coverage produced by more vigorous convection (the opposite occurred in SST−). As a consequence, the surface downward radiation was approximately the same in CONTROL, SST+, and SST−.

1. Introduction

Since tropical convection plays a determinant role in the global atmospheric circulation, it is crucial to understand the driving mechanisms for deep convection and the feedbacks associated with it. This is one of the goals of several studies related to the Tropical Ocean Global Atmosphere (TOGA) Coupled Ocean–Atmosphere Response Experiment (COARE).

One inherent characteristic of convection is that it is a multiscale process, from its large-scale organization on spatial scales of thousands of kilometers and timescales of several weeks to months, down to microphysical processes that occur on spatial scales of microns and timescales of less than 1 s. The complex interaction among large-scale, mesoscale, cloud-scale, and microphysical processes makes it virtually impossible to explicitly model all those processes in the same context. For instance, the highest resolution general circulation models and numerical weather prediction models cannot resolve small-scale phenomena such as the individual convective drafts that in fact determine the convective fluxes. Such subgrid-scale processes, thus, have to be parameterized.

Of course, representing the collective effects of a population of convective elements is not trivial. Different methodologies have been proposed to represent cumulus clouds in large-scale (and mesoscale) models, but recently it has been recognized that cloud-resolving models (CRMs) can be a useful tool to construct physically based parameterizations (e.g., Moncrieff et al. 1997).

Several studies based on cloud-resolving simulations of tropical convection using data from experiments such as TOGA COARE or Global Atmospheric Research Program (GARP) Atlantic Tropical Experiment (GATE) have been published recently. Wang et al. (1996) used the Goddard Cumulus Ensemble model and the TOGA COARE bulk flux algorithm (Fairall et al. 1996) to simulate the development of a squall line during COARE. The same case was studied by Trier et al. (1996). Grabowski et al. (1996) simulated different convective regimes during GATE using an anelastic cloud model (Clark 1977, 1979). Wu et al. (1998) performed a 39-day simulation of cloud systems formed during TOGA COARE between 5 December 1992 and 12 January 1993. Liu and Moncrieff (1998) performed two-dimensional CRM simulations to investigate the diurnal cycle of tropical oceanic convection.Grabowski et al. (1998, 1999) investigated cloud-resolving model sensitivities for the GATE case.

As pointed out by Yuter and Houze (1998), the nature

Corresponding author address: Dr. Alexandre A. Costa, Laboratório de Fisica de Nuvens e Mesoescala–LFNM Departamento de Fisca–UFC, Caixa Postal 6030, Campus do Pici, 60455-760 Fortaleza-CE, Brazil.
E-mail: alex@fisica.ufc.br

© 2001 American Meteorological Society

TABLE 1. Microphysical settings. For a given hydrometeor category, the number concentration can be user-specified, predicted, or diagnosed from the predicted mixing ratio and a user-specified mean diameter. A width parameter for the generalized gamma distribution is also specified (see Walko et al. 1995).

Category	Concentration scheme	Specified concentration	Specified mean diameter	Specified width parameter
Cloud water	Specified concentration	100 cm^{-3}	—	2
Rainwater	Specified mean diameter	—	1 mm	2
Pristine ice	Prognostic concentration	—	—	2
Snow	Specified mean diameter	—	1 mm	2
Aggregates	Specified mean diameter	—	1 mm	2
Graupel	Specified mean diameter	—	1 mm	2
Hail	Specified mean diameter	—	3 mm	2

of the convective activity over the western Pacific is variable, including shallow cumulus, vigorous cumulonimbus clouds, deep cloud clusters, and long-lived convective systems called ''superclusters.'' The dominant form of the organization of convection clearly depends on the environmental conditions, especially on the large-scale forcing. It is well known that the environmental shear, in particular, is very important in determining the way convection develops (e.g., Nicholls et al. 1988; LeMone et al. 1998).

Along with the large scale, surface forcing is an important factor to determine the evolution of cloud systems. Over the Tropics, especially over the ocean, air–sea interaction processes are recognized as a key factor driving convection. It is well known that the atmosphere responds to the heat flux at the surface, which is a function of the sea surface temperature (SST). At least on a large scale, rising motion tends to occur over warmer SSTs while sinking motion is expected over colder SSTs. Although such a relation between SST and tropical convection is recognized to exist (e.g., Webster 1994), the actual mechanisms by which the surface forcing impacts the organization of cloud systems have not been sufficiently explored.

Several theories have been proposed to explain how convection and SSTs are related in the Tropics, and many of them are based on radiational and/or evaporational regulation of the upper-ocean temperatures. Ramanathan and Collins (1991) proposed that thick cirrus clouds formed in association with deep convection eventually shield the sea surface from the solar radiation and thereby regulate the SSTs (''thermostat'' hypothesis). However, satellite data analysis by Fu et al. (1992) showed no evidence of a relationship between SST variations and cirrus cloud changes. They concluded that the large-scale circulation governs the evolution of the cirrus field. Recent cloud-resolving simulations by Wu and Moncrieff (1999) support this conclusion, which suggests that CRMs can be a valid tool to address the issue of SST regulation. However, although contributing important insights on the dependence of the cloud and water vapor feedbacks on SSTs, the results by Wu and Moncrieff (1999) still leave many questions. For instance, how do variations in the SST field influence the characteristics of cloud systems that are important to the surface radiative budget, such as cloud cover?

Numerical studies of stratocumulus to cumulus transition show that enhanced surface fluxes associated with warming SSTs can have a dramatic effect on the dynamics of the marine stratocumulus layer (Krueger et al. 1995; Wyant et al. 1997). In those studies, it has been shown that CRMs and/or large eddy simulation models are able to represent cumulus convection and small cloud coverage associated with warm SSTs, and large cloud coverage and stratiform clouds connected to cold SSTs. Of course, both the horizontal and vertical scales involved in the deep convective and the marine stratocumulus regimes are not the same. However, despite such a difference, one could ask, is tropical deep convection influenced in a similar manner by a scenario of SST warming or cooling?

The purpose of this paper is to use a cloud-resolving model to explore sensitivities of simulated cloud systems to variations in the SST. In section 2, the numerical model and the numerical experiment setup are described. In section 3, the observations relative to the period of simulation are shown. In section 4, results of the control simulation, in which the CRM was forced by the observed, averaged SST, are presented, and compared to the observations. In section 5, sensitivities of the simulated cloud systems to a warming or cooling of the SST are explored. A summary and concluding remarks are presented in section 6.

2. Cloud-resolving model

The model used for this study is a two-dimensional, cloud-resolving version of the Regional Atmospheric Modeling System (Pielke et al. 1992). Forward-in-time advection is used for scalars and a leapfrog scheme is adopted to the advection of velocity. The one-moment bulk microphysics includes seven categories of hydrometeors: cloud water, rainwater, pristine ice, snow, aggregates, graupel, and hail or frozen raindrops (Walko et al. 1995). The microphysical settings used in our simulations are described in Table 1. A two-stream radiative scheme, coupled to the microphysics, and comprising three bands of shortwave and five bands of long-

wave radiation (Harrington 1997; Olsson et al. 1998) is used. The surface parameterization is that of Louis et al. (1981), in which the fluxes are computed as a function of the roughness length, the Richardson number, the wind speed, and the differences of temperature and moisture between the air and the surface. A simple deformation-K closure (Smagorinsky 1963), in which the influences of the Richardson number (Lilly 1962) and the Brunt–Väisälä frequency (Hill 1974) are considered, was used to represent subgrid-scale turbulence.

The model setup generally followed that used for case 2 of the Global Energy and Water Cycle Experiment (GEWEX) Cloud Systems Study (GCSS) Working Group 4 (Moncrieff et al. 1997). The horizontal grid contains 512 points, with a grid spacing of 1 km and the vertical grid consists of 50 points with variable resolution (100–500-m grid spacing). A timestep of 10 s was used. Lateral boundary conditions were cyclic.

Large-scale forcing is applied following the approach described by Grabowski et al. (1996): the domain-averaged horizontal winds are nudged toward the observed values, and a contribution due to horizontal and vertical advective tendencies is added to the temperature and moisture fields.

Although two-dimensional cloud-resolving simulations of convection have shortcomings (the three-dimensional structure of cloud systems cannot be represented and downdrafts tend to be exaggerated because of the lack of a degree of freedom), it has been shown that their statistics are very close to those produced by full three-dimensional models. Tao et al. (1987) and Grabowski et al. (1998) showed that the mean dynamic, thermodynamic, and cloud fields were very similar in their 2D and 3D simulations. Also, the model intercomparison performed by the GCSS Working Group 4 showed that the several 2D CRMs and the only 3D CRM exhibited similar behaviors (Krueger and Lazarus 1999). Hence, despite the obvious limitations, two-dimensional simulations are valid tools to investigate sensitivities on cloud-resolving simulations of convection.

3. Observations

One of the most striking tropical wavelike phenomena is the 30–60-day eastward propagating oscillation (the intraseasonal oscillation, or ISO), first detected by Madden and Julian (1971). During the COARE intensive observing period (IOP), three westerly wind bursts (WWBs) associated with the ISO were observed. As pointed out by Cronin and McPhaden (1997), WWBs can strongly alter the heat budget over the western Pacific warm pool (WPWP), since dramatic changes in radiative and turbulent heat fluxes, as well as in oceanic mixing and advection, are often observed in association with them. From COARE IOP observations, Lin and Johnson (1996) found that active convection and heavy precipitation commonly occur 1–3 weeks prior to the peak WWBs.

In contrast with the approach of Wu and Moncrieff (1999) (who used idealized long-term simulations to investigate the influence of SSTs over tropical convection), we examined a real case, already described in the literature, in which deep convection was almost continuosly sustained by strong large-scale ascending motion and moisture convergence. The case studied in this paper is the evolution of the cloud systems between 19 and 26 December 1992 during a WWB event (case 2 of the GCSS Working Group 4; Moncrieff et al. 1997). The large-scale forcing for that period was constructed from the analyzed TOGA COARE data (Lin and Johnson 1996), obtained from soundings over the COARE intensive flux array (IFA). Figure 1 shows the evolution of the zonal wind (Fig. 1a), the vertical velocity in pressure coordinates (Fig. 1b), and the large-scale advective tendencies of temperature (Fig. 1c) and moisture (Fig. 1d), for that period.

As can be seen in Fig. 1a, near-surface westerlies peak on 22 December. Large-scale rising motion prevails during most of the 7-day period, with the exception of 23 and 25 December. Peaks of large-scale advective cooling and moistening occurred at altitudes about 6–7 km, on 20, 21, 22, and 24 December. As a result, significant convective activity, generating warming and drying (Q1 and Q2, not shown) occurred during most of the period, again with the exception of 23 and 25 December.

Between 19 and 26 December 1992, the SSTs experienced a general cooling trend, due to the strong surface fluxes associated with the WWB. The evolution of the average SST over the IFA during such a period is depicted in Fig. 2. In every 6-h period, a simple linear interpolation was used to obtain the SST to force the CRM at each timestep

4. Control simulation

In the control simulation, hereafter referred to only as CONTROL, the cloud-resolving model was forced by the actual observed SST (average over COARE IFA).

As in the other simulations, the model was initialized with a homogeneous sounding, corresponding to the average winds, temperature, and water vapor mixing ratio over the IFA at 0000 UTC 19 December 1992. In order to create inhomogeneities in the model atmospheric variables, a random perturbation with a 1-K amplitude was applied to the air temperature field during the first hour of simulation.

a. Comparison with observations

In general, the cloud-resolving model was able to reproduce the observed fields, shown in the previous section. Since the model winds are systematically nudged toward the observed values, very good agreement was obtained between both zonal and meridional simulated wind components and the corresponding observations.

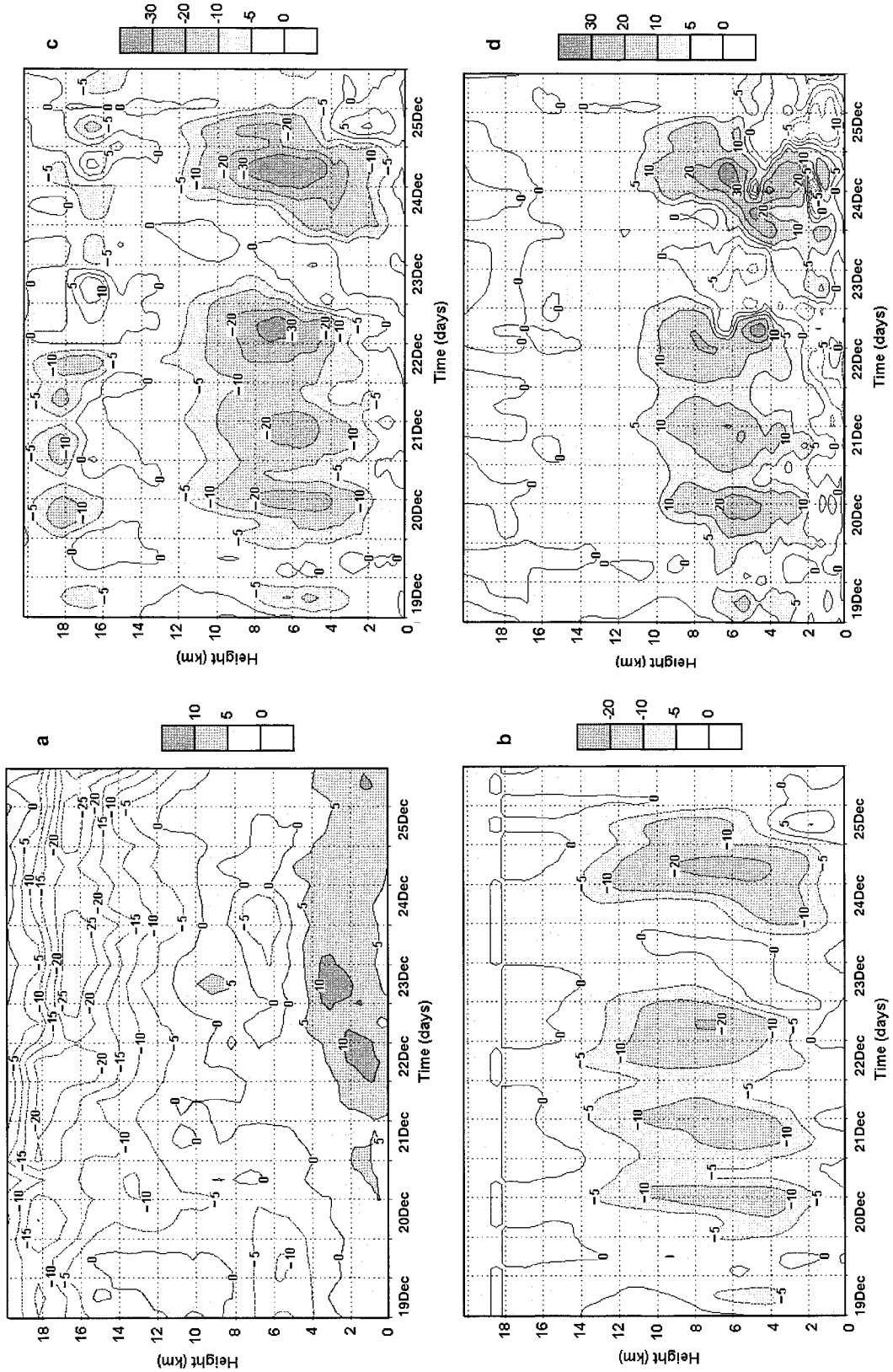

FIG. 1. (a) Observed zonal wind, in m s^{-1} (b) omega, in mb h^{-1}; (c) temperature advection, in K day^{-1}; and (d) water vapor mixing ratio advection, multiplied L/c_p in K day^{-1}. (a) Westerlies, (b) ascending motion, (c) cooling, and (d) moistening are in gray scale. All fields are averages over COARE IFA between 19 and 26 Dec 1992.

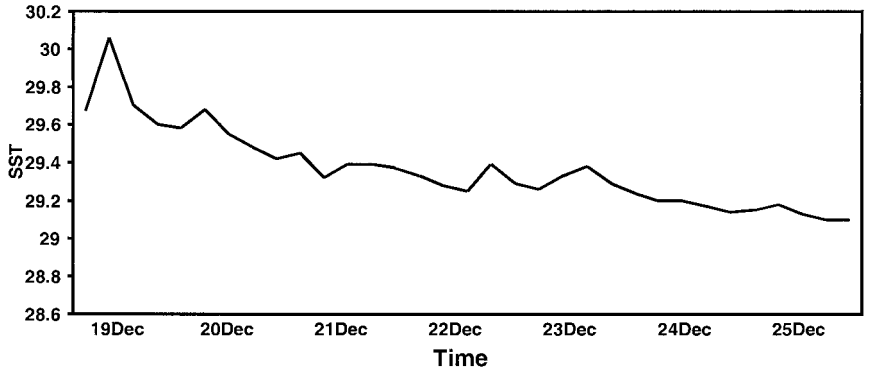

FIG. 2. Observed COARE IFA average SST, in °C, between 19 and 26 Dec 1992.

Departures from the modeled temperature and moisture fields from the observations demonstrate one of the weaknesses of the present approach. A dry, cold bias developed in most of the troposphere, similar to that found in the model intercomparison project conducted by the GCSS Working Group 4 for the same TOGA COARE case (Krueger 1997; Krueger and Lazarus 1999). Differences between the modeled and observed temperature and water vapor mixing ratio at the end of the 7-day simulation are shown in Fig. 3. A comparable drift toward a colder troposphere was found by other authors who performed similar simulations (Krueger and Lazarus 1999; Su et al. 1999, hereafter SCB). Temperature and moisture biases were also reported in cloud-ensemble simulations for different cases, as shown in the works by Grabowski et al. (1996) and Wu et al. (1998). Grabowski et al. (1996) propose that biases can develop in association with the lack of a prescribed large-scale advective forcing of hydrometeors. Also, imperfections in the large-scale forcing can generate departures from the observations (e.g., SCB).

Wu et al. (1998) show that if a relaxation term is

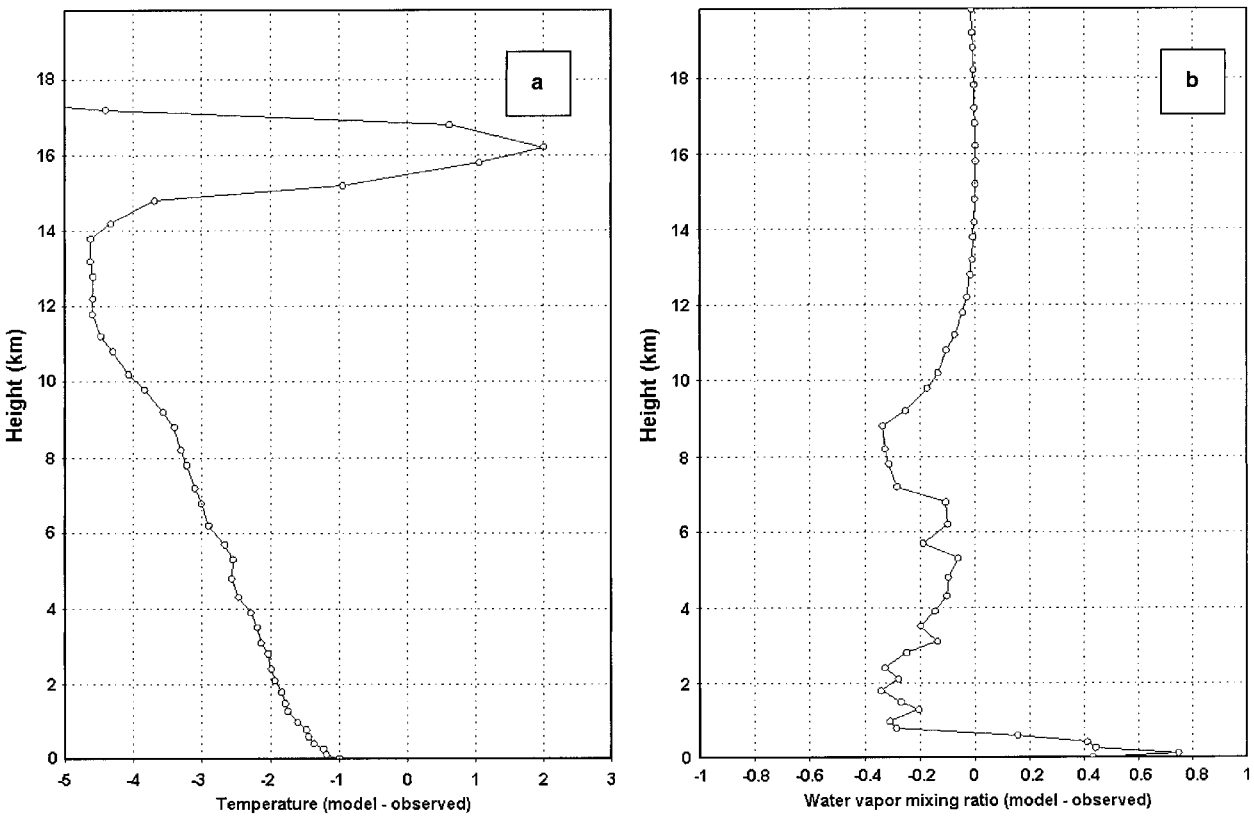

FIG. 3. Differences between the modeled and observed temperature, in °C (a) and water vapor mixing ratio, in g kg^{-1} (b) at the end of the simulation.

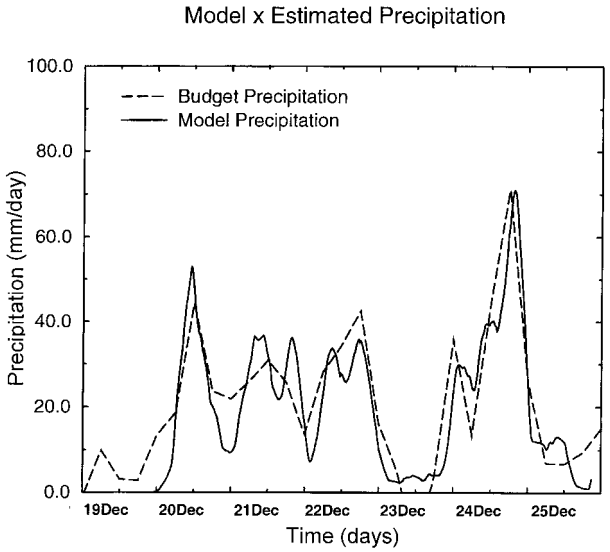

FIG. 4. Model vs ''observed'' (estimated from COARE IFA moisture budgets) precipitation, in mm h^{-1}.

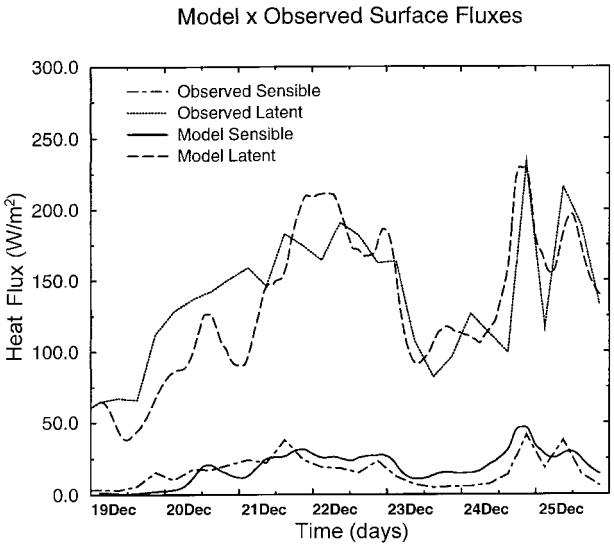

FIG. 5. Model vs observed surface heat fluxes, in W m^{-2}.

added to the large-scale temperature and moisture forcing there is an improvement in the agreement between modeled and observed fields, no matter what the actual cause of the biases is. Such a nudging term was not introduced in our simulations, though. The major goal of the present study is not to reproduce the observed fields using the CRM, but to explore sensitivities. Hence, in order to maintain simplicity, as well as to reduce the constraints that could limit the degrees of freedom in the model and might obscure the model sensitivities, no nudging was applied to the temperature and moisture fields.

The key trends in the surface precipitation were well reproduced, and the quantitative agreement between the observations and the modeled rainfall was good, as shown in Fig. 4, which compares the modeled rainfall with the one estimated from the COARE IFA budget. Of course, such agreement was expected, based on the fact that the IFA precipitation was estimated from budget calculations using the same large-scale fields that drive the CRM. The average budget precipitation for the 6-day period between 20 and 26 December was 21.9 mm day^{-1}, while the corresponding average modeled precipitation was 21.2 mm day^{-1}. 19 December was excluded from the calculation of the averaged cloud and precipitation fields, because the model required about 23 h to produce clouds (in the form of a midlevel stratiform deck) and about 26 h to generate significant precipitation at the surface.

The surface heat fluxes were, in general, accurately simulated by the CRM (see Fig. 5). The 7-day averaged model fluxes were 18.6 W m^{-2} (sensible) and 132.8 W m^{-2} (latent), while the corresponding observed values were 16.0 W m^{-2} (sensible) and 137.8 W m^{-2} (latent). All major trends were captured, especially at the end of the simulation. Despite the limitations of a 2D CRM, our results concerning the surface precipitation and the surface heat fluxes are actually in better agreement with the observations than the ones obtained by SCB using a 3D CRM.

b. Condensate fields, cloud coverage

According to observations (e.g., Wu et al. 1998), the region of COARE IFA was mostly covered by clouds between 20 and 25 December 1992, with particularly low values of the cloud-top temperature on 20–22 and 24 December.

Figure 6 shows the time evolution of the domain-averaged total condensate mixing ratio for the simulation period and Fig. 7 represents the 6-day averages of the total condensate, cloud water, rainwater, low-density ice, and high-density ice mixing ratios. In Fig. 6, deep convection developed on the second day of simulation and lasted until the end of the fourth day, when shallow cumuli and cirrus clouds (produced by previous deep convection) predominated. Deep convection returned on the sixth day, lasting until close to the end of the simulation. In general, the present results agree with other modeling studies of the same case (e.g., SCB). In contrast with the total condensate, which is constrained by the imposed large-scale forcing, the distribution of the water substance among different categories (cloud water, rainwater, and ice species) depends on the microphysical parameterization and its free parameters. For instance, our results have significant departures from SCB that used a microphysical parameterization in which graupel was not included. For the current microphysical parameters, low-density ice (pristine ice, snow, and aggregates) dominated the condensate field in our simulations and the presence of graupel and hail was relatively small during the entire simulation period.

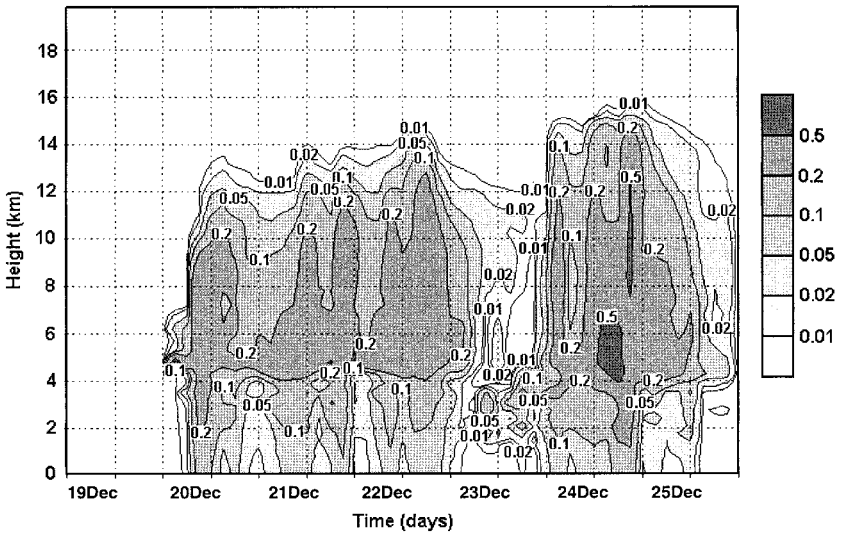

FIG. 6. Model total condensate mixing ratio, 3-h running domain average (CONTROL), in g kg^{-1}.

Figure 8 shows the 6-day average of the domain-averaged cloud fractional area (a cloudy grid box is defined as the one containing at least 0.01 g kg^{-1} of cloud water plus cloud ice). As in the GATE simulations of Grabowski et al. (1998), a bimodal distribution of cloud coverage occurs in CONTROL, with a primary peak of cloudiness at high levels (approximately 14 km) and a secondary peak near the melting level (about 5 km). However, for the present simulated TOGA COARE

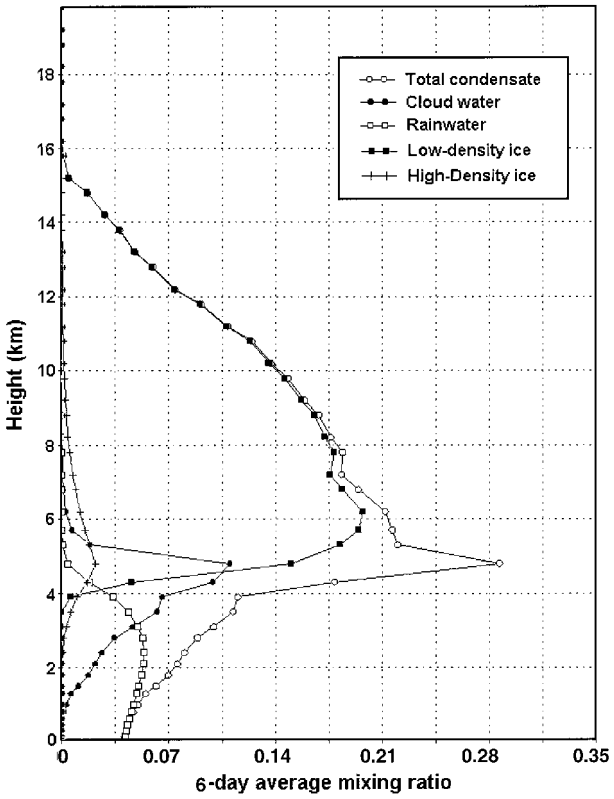

FIG. 7. 6-day (between 20 and 26 Dec) averaged mixing ratios (CONTROL) in g kg^{-1}.

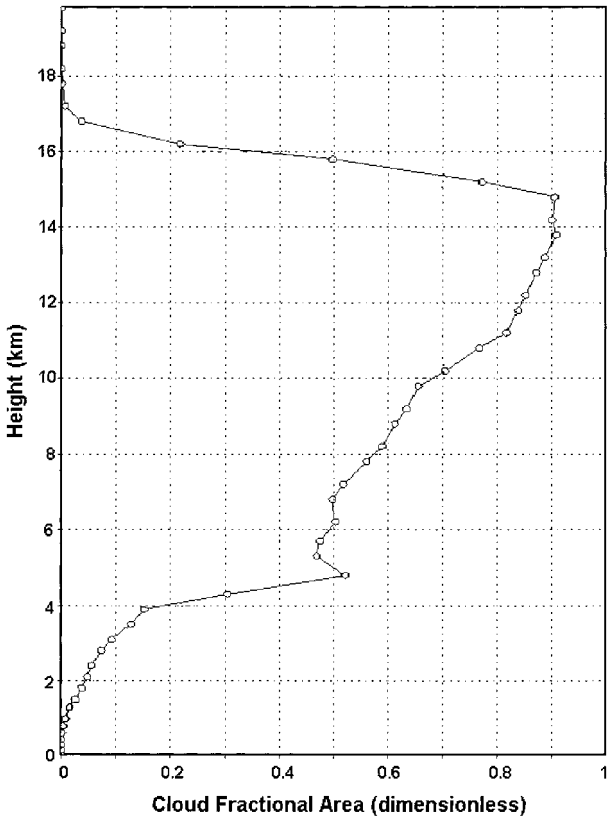

FIG. 8. 6-day (between 20 and 26 Dec) averaged cloud fractional area (CONTROL).

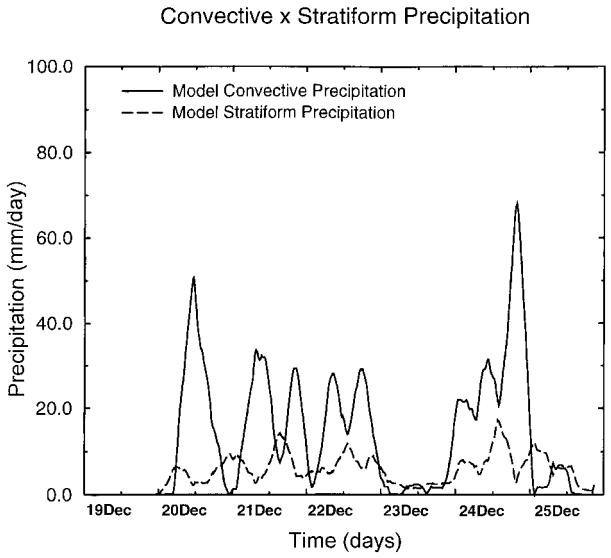

FIG. 9. Convective and stratiform precipitation, 3-h running domain average (CONTROL), in mm day^{-1}.

case, both peaks were more intense, and the high-level peak is located at a more elevated altitude than in the GATE simulations referred to above.

c. Convective–stratiform partition, cloud mass flux

One important issue about the development of parameterizations for GCMs is the separation between the convective and the stratiform parts of cloud systems. In cloud-resolving simulations such a partition can be assessed explicitly [see Xu (1995) and Alexander and Cotton (1998)].

Figure 9 shows the time evolution of the convective and stratiform precipitation in CONTROL. Table 2 shows the 6-day averaged model convective and stratiform precipitation and convective and stratiform fractional area. Although ''convective columns'' cover less area than ''stratiform columns'' (as expected), the larger contribution to the total precipitation came from the convective elements of the cloud systems, due to the heavy rainfall produced by them. Stratiform precipitation and convective precipitation are out of phase, with stratiform rain generally following the occurrence of convective events. The obvious exception in Fig. 9 is the first occurrence of stratiform precipitation, associated with the model spinup.

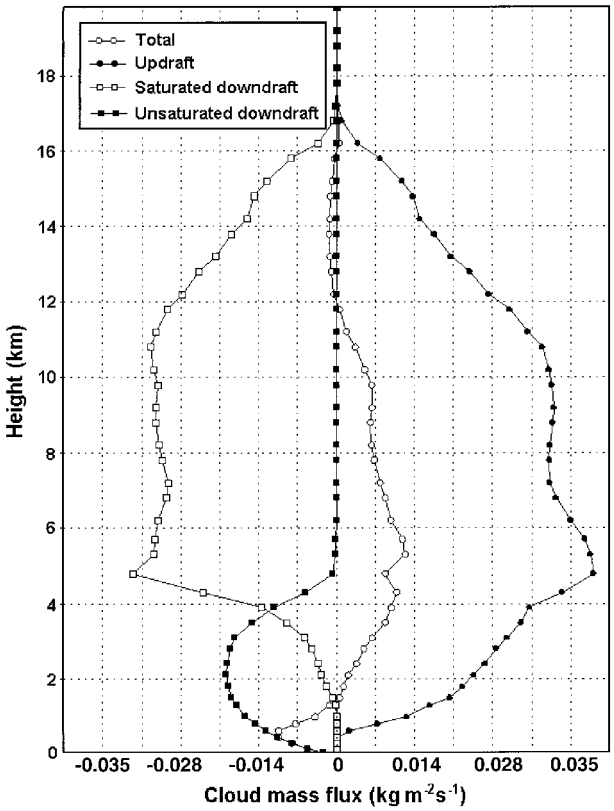

FIG. 10. 6-day (between 20 and 26 Dec) averaged cloud mass fluxes (CONTROL) in kg m^{-2} s^{-1}.

Figure 10 represents the 7-day average of the total, updraft, saturated downdraft, and unsaturated downdraft cloud mass flux in CONTROL. In the computation of the total cloud mass flux, the contribution of unsaturated downdrafts, which occur mostly in association with rainfall, was incorporated. Such a component is the major contributor to the downdraft cloud mass flux below cloud base. It produces negative values of the total cloud mass flux at low levels, which are quite evident in Fig. 10.

TABLE 2. 6-day averages of the convective and stratiform precipitation, convective, and stratiform fractional area in CONTROL.

Variable	CONTROL	ENS1	ENS2	ENS3	ENS4	Standard deviation
Total precipitation (mm day^{-1})	21.19	21.22	21.02	20.94	21.01	0.11 (0.5%)
Convective precipitation (mm day^{-1})	15.25	15.01	15.16	14.77	15.03	0.16 (1.1%)
Stratiform precipitation (mm day^{-1})	5.94	6.21	5.86	6.17	5.98	0.14 (2.2%)
Latent heat flux (W m^{-2})	132.81	134.87	133.25	132.31	133.51	0.74 (0.6%)
Sensible heat flux (W m^{-2})	18.63	18.57	18.73	18.49	18.47	0.10 (0.5%)
Downward solar radiation (W m^{-2})	122.62	118.44	125.81	136.19	132.20	3.45 (2.7%)
Downward IR radiation (W m^{-2})	412.00	412.87	413.66	414.05	412.52	0.75 (0.2%)
Upward solar radiation (W m^{-2})	7.36	7.11	7.55	8.17	7.93	0.21 (2.7%)
Upward IR radiation (W m^{-2})	469.45	469.45	469.45	469.45	469.45	0.00 (0.0%)

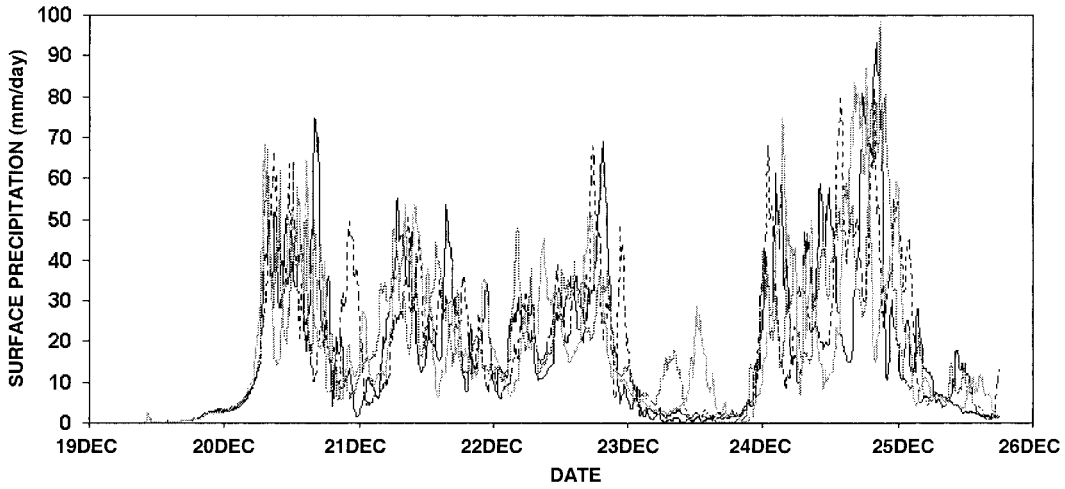

FIG. 11. Time evolution of the domain-averaged surface precipitation, in mm day^{-1}, between 19 and 26 Dec 1992, for the simulations ENS1 (black line), ENS2 (dotted line), ENS3 (dashed line), and ENS4 (gray line).

d. Statistical significance

In order to verify the statistical significance of CONTROL a small ensemble of similar runs was constructed. The difference among CONTROL and those four runs (hereafter referred to as ENS1, ENS2, ENS3, and ENS4) resided in the random temperature perturbations imposed to the temperature field. As will be demonstrated in this section, despite the differences in the individual evolution of each one of those simulations, their statistics are strikingly similar.

In general, the evolution of the domain-averaged precipitation-related quantities looked alike. This is expected, due to the fact that the tropical atmosphere tends to adjust itself to a profile close to the moist adiabatic, consuming convective available potential energy (CAPE) and producing precipitation. Hence, the statistical properties of convection (which accounts for the consumption of CAPE and the consequent ''quasi-moist adiabatic adjustment'') must obey the imposed large-scale forcing, regardless of the actual evolution of the convective systems. Particularly in a case of strong forcing on the large scale, multiday CRM simulations are expected to be robust in terms of their statistics.

The evolution of the domain-averaged total surface precipitation in ENS1 to ENS4 is shown in Fig. 11. The strong temporal variability shown in Fig. 11, contrasting with the much smoother 6-h moving average of the total precipitation in CONTROL shown in Fig. 4, is a well-known characteristic of two-dimensional CRM simulations of convection (e.g., Grabowski et al. 1998). A similar variability appears in other variables, such as convective and stratiform precipitation, latent and sensible heat fluxes, radiative fluxes, etc. In an average sense, however, those variables exhibited very close values in ENS1 to ENS4, as well as in CONTROL, as shown in Table 3.

TABLE 3. Time average of some domain-averaged quantities for simulations CONTROL and ENS1 to ENS4. Precipitation-related variables were averaged between 20 and 26 Dec. Other variables were averaged in the entire 7-day simulation period. The value in parenthesis shown in the last column is the percentage of the standard deviation with respect to the average for the five simulations.

Convective precipitation	15.3 mm day^{-1} (72.2% of the total)
Stratiform precipitation	5.9 mm day^{-1} (27.8% of the total)
Total precipitation	21.2 mm day^{-1}
Convective fractional area	0.3103
Stratiform fractional area	0.4234
Total rainy fractional area	0.7337

5. Sensitivity to SST increase or decrease

Two sensitivity experiments were performed in which the SST trend shown in Fig. 2 was maintained, but the actual SST value was reduced (SST− simulation) or increased (SST+ simulation) by 1°C. In both simulations, as in CONTROL, the sea surface temperature is spatially homogeneous.

The imposed atmospheric large-scale forcing in SST− and SST+ was the same used to drive the CRM in CONTROL, although in reality the large-scale circulation depends on the SST field. Contrary to intuition, Betts and Ridgway (1989) and Betts (1998) point out that the mass circulation in the Tropics decreases for increasing SSTs. As shown by Wu and Moncrieff (1999), there was no obvious relationship between the evolution of the SST and the thermal large-scale forcing over the TOGA COARE IFA. However, utilization of the same large-scale forcing to drive all simulations, although not completely realistic, is useful. It allows us to evaluate the sensitivity of the organization of cloud systems with respect to SST at the time- and spatial scales of the convective systems themselves. Indeed, the use of the same large-scale forcing compelled the cloud systems in both SST− and SST+ to behave close to the ones in CONTROL.

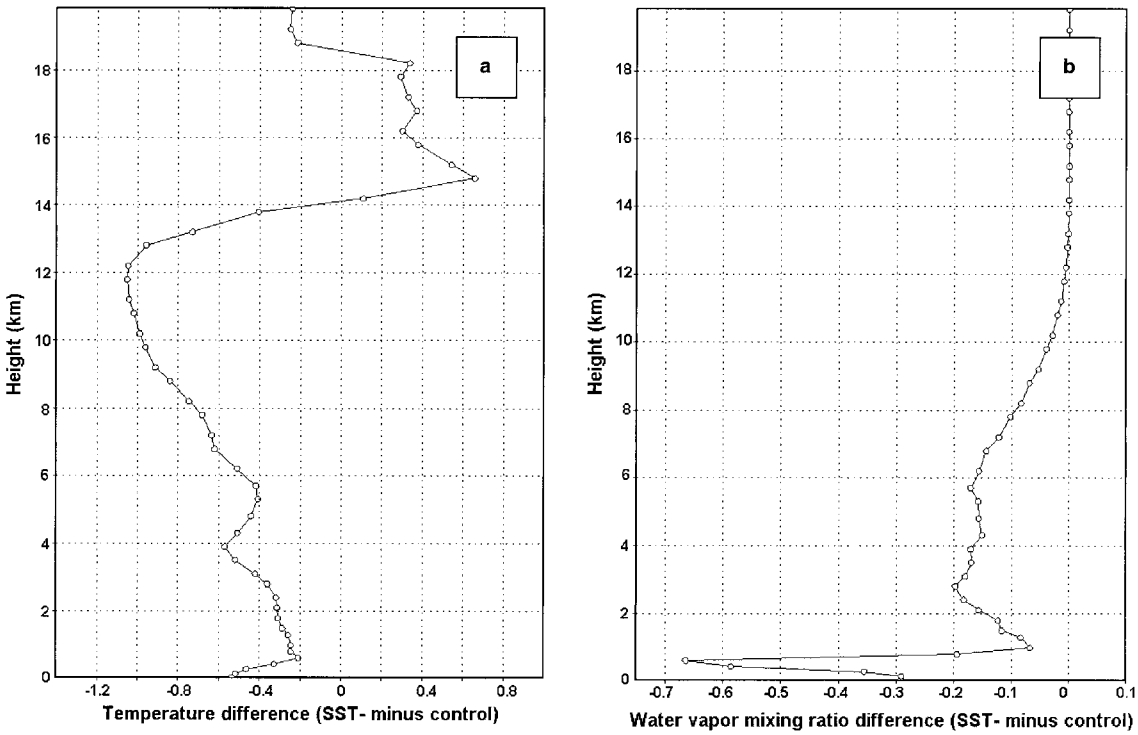

FIG. 12. 6-day (between 20 and 26 Dec) averaged difference between SST− and CONTROL: (a) temperature, in °C, and (b) water vapor mixing ratio, in g kg^{-1}.

a. SST− simulation

The cold, dry bias described earlier was exacerbated in this simulation, a consequence of reduced surface heating and moistening. Figure 12 shows the difference between the model temperature (Fig. 12a) and water vapor mixing ratio (Fig. 12b) in simulations SST− and CONTROL, averaged over the 6-day period between 20 and 26 December. Temperature differences larger than 1° and mixing ratio differences close to 1g kg^{-1} were found.

The evolution of the domain-averaged total condensate field is quite similar to that in CONTROL, which suggests that the large-scale forcing plays a major role in determining the characteristics of tropical cloud systems. Some differences between the cloud systems in SST− and CONTROL were observed, though. The total cloud mass flux is smaller by about 3% in SST−. Cloud water maxima are more persistent, rainwater peaks are slightly less pronounced, and the amount of ice is smaller in SST− than in CONTROL (figure not shown). The 6-day averaged total condensate field and cloud fractional area in SST− exhibit some important departures from what was observed in CONTROL. There was an excess of condensate in SST−, in the form of cloud water, from above the boundary layer up to the melting level, that is, on average, as high as 0.044 g kg^{-1}, which is very significant in terms of a domain average. In contrast, in upper levels, SST− exhibited a deficit of low-density ice, of the order of 0.026 g kg^{-1} at 13 km (Fig. 13a).

In terms of cloud coverage, at most levels there were more clouds in SST− than in CONTROL. Below the melting level, at approximately 4.5-km height, the cloud fraction in SST− surpassed the one in CONTROL by as much as 10%. In contrast, at high levels, due to the weakened convective transport, less ice was detrained from the top of the cloud systems, and the cloud fractional area associated with anvil clouds was reduced by more than 4%.

b. SST+ simulation

Most of the differences between SST− and CONTROL also occurred between SST+ and CONTROL, with an opposite sign. The cold, dry bias was reduced in SST+ (Fig. 14). Cloud water maxima were less steady and rainwater maxima were sharper. On average, the high-density ice mixing ratio (grauple and hail), although still small, was greater in SST+ than in SST− and CONTROL. Aspects of the average behavior of the cloud systems in SST+ are depicted in Fig. 15. In the lowest 3 km, SST+ showed more condensate than CONTROL (maximum excess of about 0.003 g kg^{-1} in the 6-day average), associated with increased rainwater. The vertical distribution of the condensate was shifted upward in SST+, as indicated by the two bipolar fea-

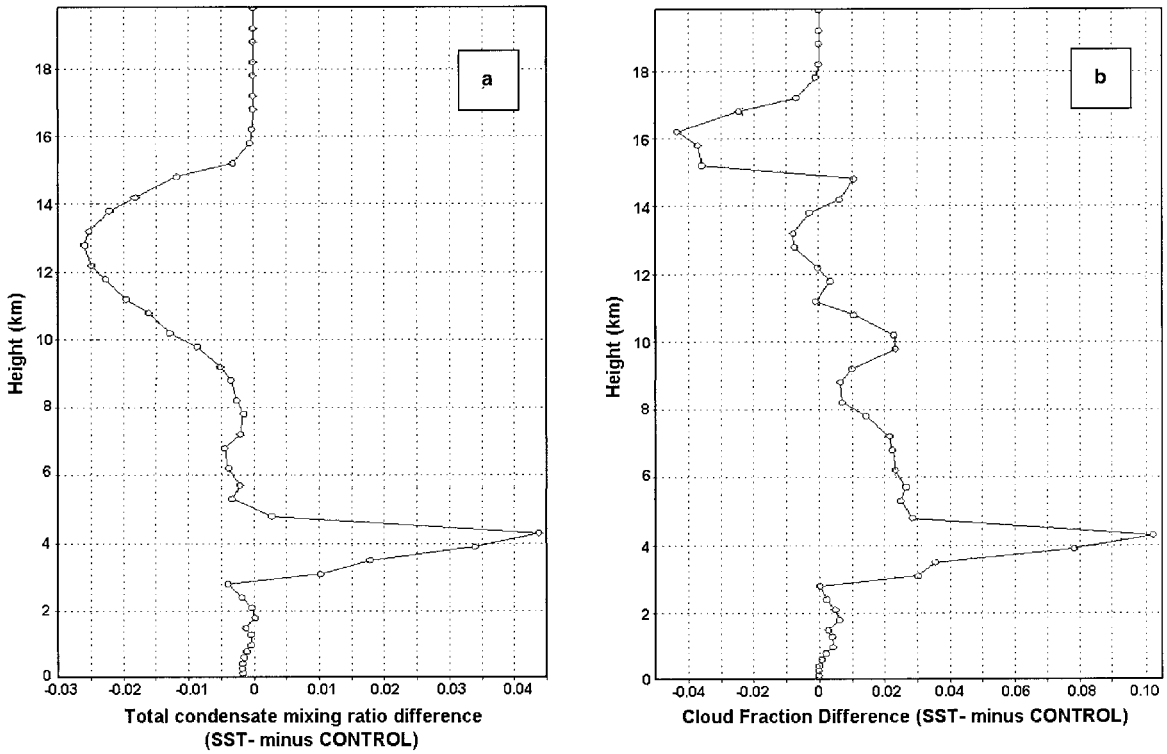

FIG. 13. 6-day (between 20 and 26 Dec) averaged difference between SST− and CONTROL: (a) total condensate mixing ratio, in g kg^{-1}, and (b) cloud fractional area, dimensionless.

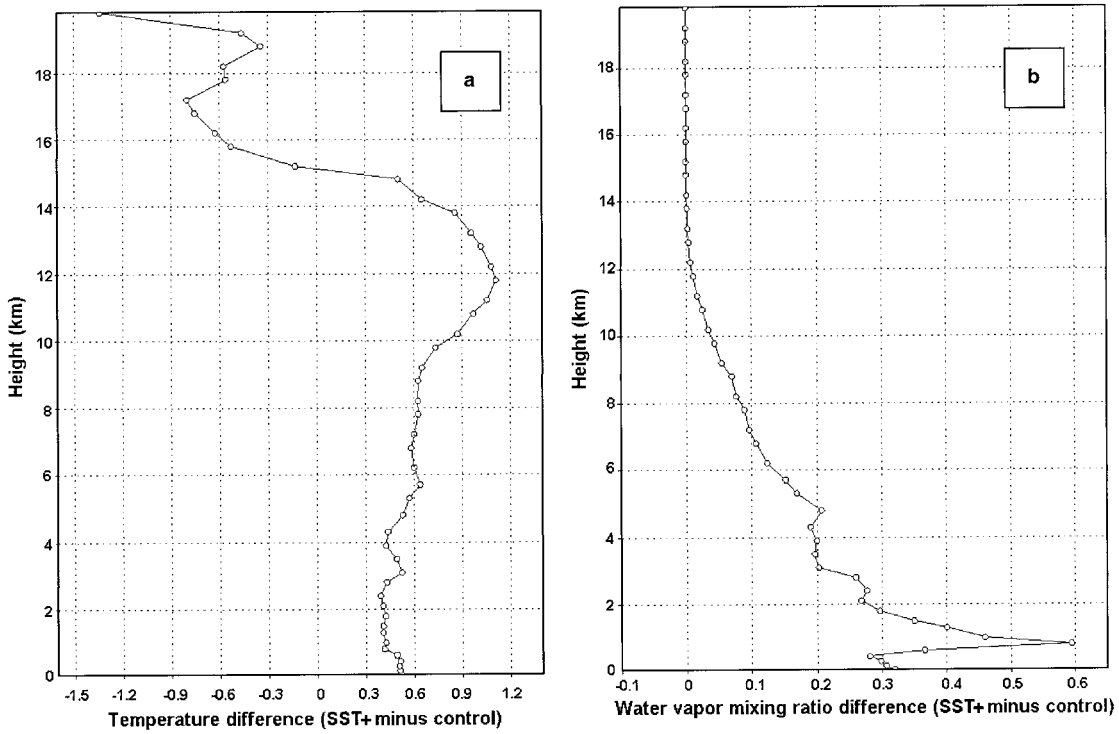

FIG. 14. Same as Fig. 12, except between SST+ and CONTROL.

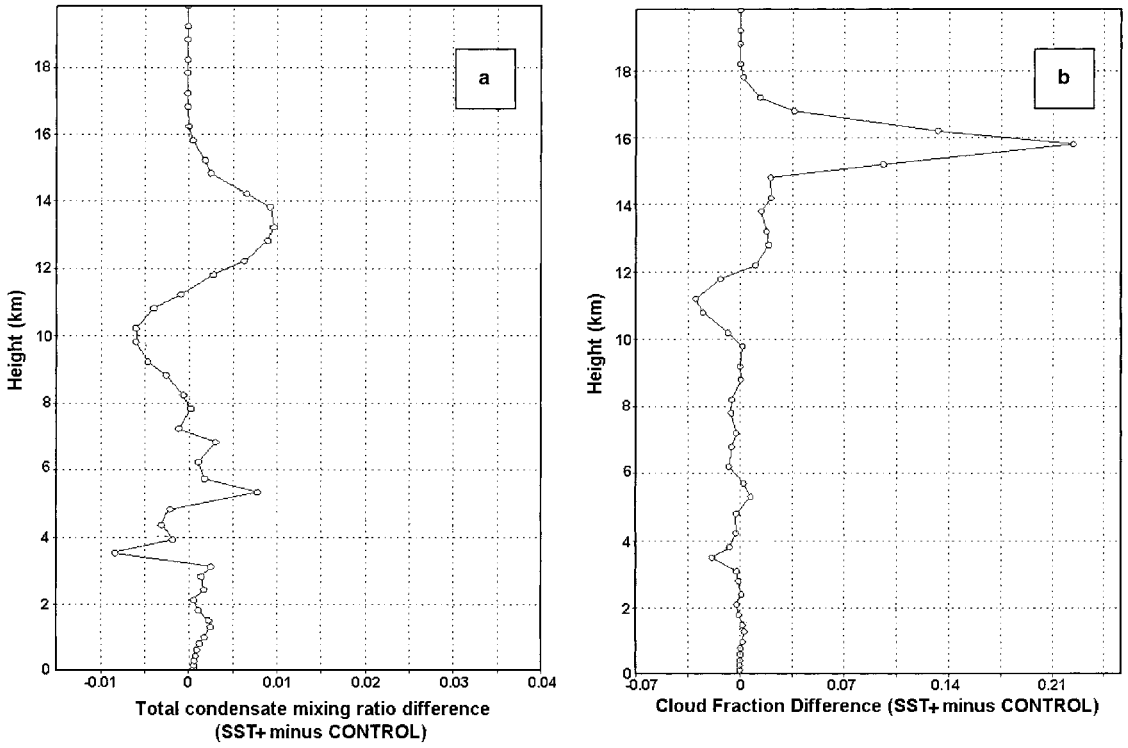

FIG. 15. Same as Fig. 13, except between SST+ and CONTROL.

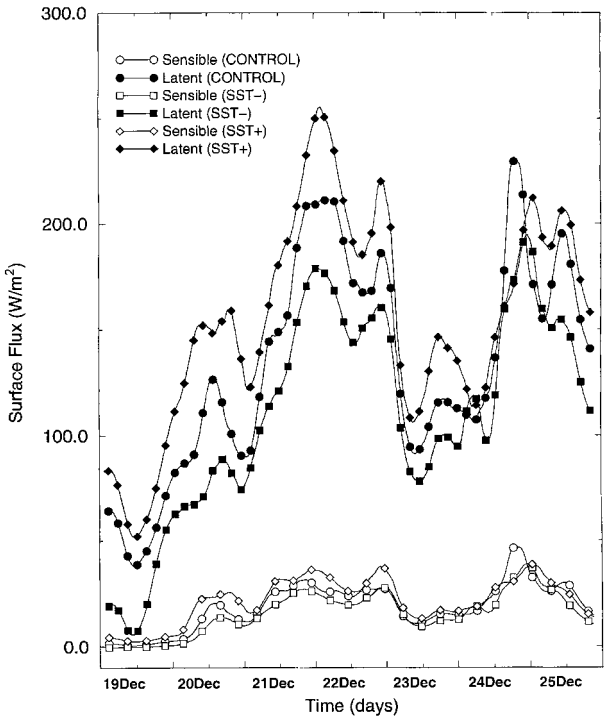

FIG. 16. Sensible and latent heat fluxes in CONTROL, SST−, and SST+, in W m^{-2}.

tures in Fig. 15a (one between about 3 and 7 km and the other from 8 to 16 km), suggesting a more efficient vertical transport of the water substance. SST+ presented about the same cloud coverage as CONTROL from the surface to 10 km, except about the 3.5-km level, where SST+ showed a deficit on the order of 2% in the cloud fractional area. More cloud coverage was found in the upper troposphere associated with more vigorous ice detrainment through anvil clouds in SST+. The average excess in the cloud fractional area aloft was as high as 18%, in contrast with the high-level cloud coverage deficit that occurred in SST−. The increased cloud fraction was not accompanied by a significant condensate excess because it was associated with cirrus clouds exhibiting very small ice–water mixing ratios.

c. Heat fluxes, convective–stratiform partition

As expected, on average both sensible and latent heat fluxes increased as the sea surface temperature increased, that is, SST+ showed the greatest fluxes, followed by CONTROL and SST− (Fig. 16). In percentage terms, such hierarchy was more obvious at the beginning of the simulated period. However, as the simulations progressed, the CRM acted to reduce the relative differences in the heat fluxes. This might suggest that the model attempted to adjust the surface fluxes to the imposed large-scale forcing when convection occurs.

CONTROL, SST−, and SST+ presented similar val-

TABLE 4. 6-day averages of the convective and stratiform precipitation, convective, and stratiform fractional area in SST− and SST+.

	SST−	SST+
Convective precipitation	14.1 mm day^{-1} (69.1% of the total)	16.6 mm day^{-1} (76.4% of the total)
Stratiform precipitation	6.3 mm day^{-1} (30.9% of the total)	5.1 mm day^{-1} (23.6% of the total)
Total precipitation	20.4 mm day^{-1}	21.7 mm day^{-1}
Convective fractional area	0.2860	0.3350
Stratiform fractional area	0.4574	0.4017
Total rainy fractional area	0.7434	0.7367

ues of total precipitation, with the total precipitation in SST+ exceeding that in SST− by less than 6%. The results show the strong constraint imposed by the prescribed large-scale forcing on the precipitation field and suggest that, for the simulated regime, there is a weak relationship between SST and precipitation rate. Such a connection may be a multistep process, involving surface parameters (such as the SST), surface fluxes, large-scale circulation, and precipitation. The results also indicate that it is the large-scale circulation that determines the precipitation rate (although the large-scale forcing itself can be affected by the surface conditions over a greater scale). This is consistent with the premise behind many cumulus parameterizations such as the Arakawa–Schubert scheme (Arakawa and Schubert 1974) as well as other schemes (Shrinivas and Suarez 1992; Wang and Randall 1996; Cheng and Arakawa 1997; Pan and Randall 1998; Ding and Randall 1998).

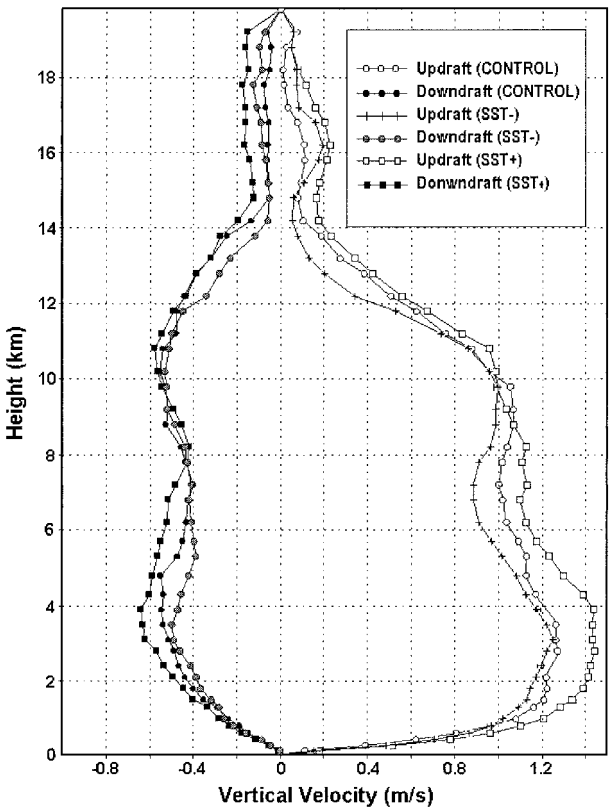

FIG. 17. 6-day (between 20 and 26 Dec) averaged core updraft and core downdraft velocities (CONTROL, SST−, and SST+). See text for details.

Despite the relative insensitivity of the precipitation to changes in the SST, differences were observed regarding precipitation production in SST− and SST+. Table 4 shows the 6-day averaged model convective and stratiform precipitation and the convective and stratiform fractional area for those two simulations. It was observed that a significant growth in the convective component of the precipitating systems occurred as the SST increased. One possible explanation is that the enhanced (suppressed) surface fluxes, associated with warmer (cooler) SSTs, can generate more (less) vigorous thermals in the boundary layer that can eventually generate more (less) deep convective elements. The more (less) pronounced subsidence related to more (less) vigorous convection and associated cloud mass fluxes account for the reduction (increase) in low-level cloud coverage in SST+ (SST−). Despite the obvious differences, these findings are similar to those by Krueger et al. (1995) and Wyant et al. (1997) in their simulations of marine stratocumulus, in which higher SSTs favored cumulus convection and inhibited the development of stratiform clouds.

In order to illustrate the differences in the updrafts and downdrafts in CONTROL, SST−, and SST+, it is appropriate to use the definition of the ''core updraft'' and ''core downdraft'' velocities. In our simulations, a ''core'' is defined as a contiguous set of model points in which the absolute value of the vertical velocity exceeds 1 m s^{-1}. The domain-averaged updraft velocity at a certain time is simply the vertical velocity averaged over the points in which it exceeds 1 m s^{-1}. If, at a given time, the vertical velocity is smaller than this value everywhere in the domain, the domain-averaged updraft velocity is set to zero. The domain-averaged downdraft velocity follows a similar definition. Figure 17 depicts the 6-day mean of the domain-averaged updraft and downdraft velocities. It is clear that more vigorous updrafts, as well as a stronger compensating subsidence, occurs in association with higher SSTs. This is consistent with a greater 7-day averaged CAPE in SST+ (1129 J kg^{-1}) and a smaller CAPE in SST− (966 J kg^{-1}), with an intermediate value found in CONTROL (1039 J kg^{-1}).

d. Radiative fluxes

Many researchers proposed that evaporative cooling and blocking of solar radiation could act as regulating

TABLE 5. 6-day averages of the net surface radiative flux and the surface downward shortwave radiative flux in SST−, SST+, and CONTROL. Positive values indicate downward flux.

Numerical experiment	7-day averaged net surface radiative flux (W m^{-2})	7-day averaged downward shortwave radiative flux (W m^{-2})	7-day averaged surface latent heat flux (W m^{-2})
CONTROL	66.8	132.2	132.9
SST−	73.4	135.2	109.2
SST+	62.6	128.0	154.7

factors for the SSTs. For instance, Ramanathan and Collins (1991) proposed that there exists a negative feedback between deep convection and SST, that is, convection developing over warm SSTs produces cirrus clouds that block the solar radiation, thereby leading to a cooling of the ocean surface. In opposition, several authors contested this ''cirrus-thermostat hypothesis'' (e.g., Fu et al. 1992; Wu and Moncrieff 1999). Questions persist regarding this subject.

Despite the uncoupled nature of every numerical experiment shown in this paper (the SSTs were always specified), the present simulations can give information regarding the SST regulation. For instance, sensitivities in the evaporation and surface radiative budget indicate how the ocean temperature could potentially change. In the present simulations, the influence of the organization of the cloud systems on the radiative budget was small (Table 5). Both the variations in the net radiative surface flux and the surface downward shortwave radiation were small compared to the changes in the surface latent heat flux. This suggests that turbulent fluxes of sensible and latent heat may be more important in regulating the SSTs than the cirrus thermostat effect. Although, in our simulations, more high-level clouds were produced as the SST increased, the radiation budget indicates that the cirrus-thermostat effect accounts for a very small part of the regulation of the SSTs in the Tropics. Also, the structure of the cloud coverage in SST+ and SST− suggests the existence of a mechanism in opposition to the cirrus thermostat; a positive boundary layer cloud feedback similar to the one found in the stratocumulus–cumulus transition regime, that is, more (less) low-level to midlevel cloud coverage being produced over colder (warmer) SSTs.

According to the present results, other factors than the blocking of solar radiation by cirrus clouds can play a more significant role to limit the values of the tropical ocean surface temperatures. Among those factors are the longwave radiation and, more important, the cooling associated with the turbulent fluxes. Considering the contribution from other mechanisms (''dynamic thermostat,'' e.g., Clement et al. 1996), the picture that emerges is of a very complex regulation mechanism for the tropical SSTs. CRM simulations coupled to an ocean model, so the surface temperature would be allowed to evolve, can provide useful information on that subject. It is clear that the construction of a comprehensive conceptual model for the SST regulation is still incomplete and will require further investigation.

6. Summary, conclusions, and future work

Two-dimensional cloud-resolving simulations of the evolution of tropical convection over the western Pacific warm pool between 19 and 26 December 1992 were performed. Results from a control simulation showed that the CRM is generally able to represent the response of cloud systems to the large-scale forcing.

Sensitivity tests were performed in order to evaluate the influence of SSTs on the behavior of the simulated cloud systems. Most of the atmospheric fields were very similar in all simulations, indicating the dominant influence of the prescribed large-scale forcing. For the case of warmer SSTs, the variation of total precipitation was smaller than would be obtained if the extra supply of moisture from the surface were totally converted to precipitation, since part of it was used to moisten the atmosphere. The enhanced evaporation, associated with warmer SSTs, contributed, in part, to increase the presence of water vapor throughout the troposphere (the opposite occurred for the case of cooler SSTs). The results reinforce the point of view that the primary driver for precipitation production is the large-scale circulation rather than the surface fluxes (although in reality the local surface forcing and the remote large-scale forcing cannot be separated). Moreover, it agrees with the baseline assumptions of several convective parameterizations, in which the precipitation is estimated based on the characteristics of the large-scale flow.

However, despite the similarities in most of the simulated fields, including the total precipitation, the simulations revealed important sensitivities in the organization of the cloud systems to the imposed SST field. A relationship was observed between the average magnitude of the surface fluxes and the manner in which the model separates the convective and stratiform components of cloud systems. For instance, the 6-day mean of the area covered by convective elements and the precipitation associated with them increased by about 17% from the simulation with cooler SSTs to the simulation with warmer SSTs, that is, more and stronger convective elements were produced as the SST increased. Also, compensating subsidence increased as the SST in-

creased, modifying the distribution of cloud coverage and total condensate.

Although more cirrus clouds formed in the simulation with larger SSTs, the amount of solar radiation that reached the surface in SST+ was approximately the same as in SST− and CONTROL, contrary to the cirrus-thermostat theory. The similar values of surface downward shortwave radiation in CONTROL, SST−, and SST+ were primarily due to the reduction (enhancement) of low-level cloud coverage in association with warmer (colder) SSTs. A similar feedback has been suggested on a larger scale in the transition between the marine stratocumulus (Sc) and trade wind cumulus (Cu) regimes. In the case of the Sc to Cu transition, a positive feedback occurs between cloud coverage and SST, such that cold (warm) SSTs help to support (destroy) stratiform clouds, increasing (reducing) the fractional cloud area, which favors further cooling (warming) of the sea surface.

Additional research is required to verify whether such a feedback also occurs in the deep convective regime or not. The present study has evident limitations; for example, constraining all the simulations by using the same large-scale forcing is not completely realistic, because the forcing actually depends on the SST. Also, because two-dimensional simulations exclude one of the natural degrees of freedom of convection, downdrafts tend to be exaggerated. Therefore, the observed differences in the convective–stratiform partition and the small impact on the radiative budget might be an artifact of applying the large-scale forcing in a two-dimensional framework. Determining the impact of the two-dimensionality can be investigated using full three-dimensional cloud-resolving simulations. However, nested-grid CRM simulations are required in order to account for the full range of dynamical interaction on multiple scales.

In the western Pacific warm pool, complex atmosphere–ocean feedbacks are established due to intricate coupling. Dramatic examples of such a coupling, associated with clouds and precipitation in the WPWP are the formation of the barrier layer (e.g., Lukas and Lindstrom 1991) and the development of a shallow warm layer (e.g., Fairall et al. 1996), responsible for significant changes in the radiative fluxes to the atmosphere. Because processes associated with atmospheric convection can modify the state of the ocean, one surmises that, in order to model the convection over the WPWP properly, a two-way communication between the atmosphere and the ocean is essential. This is the major motivation in coupling an upper-ocean model (UOM) to a CRM, in agreement with the proposition by Moncrieff et al. (1997) who suggest that coupling CRMs to ocean models is important. Studies using a coupled CRM–UOM to investigate TOGA COARE cases are currently being carried out.

In our point of view, the use of both a coupled and an uncoupled CRM to study atmospheric convection over tropical oceans can find at least two major applications in the near future. First, cloud-resolving simulations will help to understand the complex air–sea feedbacks that operate in association with tropical convection, with an explicit representation of various physical processes, as radiative transfer, microphysical phenomena, turbulent transport, and—in the case of coupled modeling—upper-ocean dynamics. Second, data from sensitivity experiments with a CRM regarding the SSTs can be used to develop parameterizations of the influence of surface processes in cloud-related quantities for large-scale models.

Acknowledgments. This research was supported by the Conselho Nacional de Desenvolvimento Científico e Tecnológico (CNPq, Brazil) and by the National Oceanic and Atmospheric Administration under Grant NA67RJ0152. The authors grateful acknowledge the valuable suggestions made by two anonymous reviewers.

REFERENCES

Alexander, G. D., and W. R. Cotton, 1998: The use of cloud-resolving simulations of mesoscale convective systems to build a mesoscale parameterization scheme. *J. Atmos. Sci.,* **55,** 2137–2161.

Arakawa, A., and W. H. Schubert, 1974: Interaction of a cumulus cloud ensemble with the large-scale environment, Part I. *J. Atmos. Sci.,* **31,** 674–701.

Betts, A. K., 1998: Climate-convection feedbacks: Some further issues—An editorial comment. *Climatic Change,* **39,** 35–38.

——, and W. Ridgway, 1989: Climatic equilibrium of the atmospheric convective boundary-layer over a tropical ocean. *J. Atmos. Sci.,* **46,** 2621–2641.

Cheng, M.-D., and A. Arakawa, 1997: Inclusion of rainwater budget and convective downdrafts in the Arakawa–Schubert cumulus parameterization. *J. Atmos. Sci.,* **54,** 1359–1378.

Clark, T. L., 1977: A small-scale dynamic model using a terrain following coordinate. *J. Comput. Phys.,* **24,** 186–215.

——, 1979: Numerical simulations with a three-dimensional cloud model: Lateral boundary condition experiments and multicellular severe storm simulations. *J. Atmos. Sci.,* **36,** 2191–2215.

Clement, A. C., R. Seager, M. A. Cane, and S. Zebiak, 1996: An ocean dynamic thermostat. *J. Climate,* **9,** 2190–2196.

Cronin, M. F., and M. J. McPhaden, 1997: The upper ocean heat balance in the western equatorial Pacific warm pool during September–December 1992. *J. Geophys. Res.,* **102,** 8533–8553.

Ding, P., and D. A. Randall, 1998: A cumulus parameterization with multiple cloud levels. *J. Geophys. Res.,* **103,** 11 341–11 353.

Fairall, C. W., E. F. Bradley, D. P. Rogers, J. B. Edson, and G. S. Young, 1996: Bulk parameterization of air-sea fluxes for Tropical Ocean–Global Atmosphere Coupled Ocean–Atmosphere Response Experiment. *J. Geophys. Res.,* **101,** 3747–3764.

Fu, R., A. D. Del Genio, W. B. Rossow, and W. T. Liu, 1992: Cirrus-cloud thermostat for tropical sea surface temperatures tested using satellite data. *Nature,* **358,** 394–397.

Grabowski, W. W., X. Wu, and M. W. Moncrieff, 1996: Cloud resolving modeling of tropical cloud systems during Phase III of GATE. Part I: Two-dimensional experiments. *J. Atmos. Sci.,* **53,** 3684–3709.

——, ——, ——, and W. D. Hall, 1998: Cloud resolving modeling of tropical cloud systems during Phase III of GATE. Part II: Effects of resolution and the third spatial dimension. *J. Atmos. Sci.,* **55,** 3264–3282.

——, ——, and ——, 1999: Cloud resolving modeling of tropical

cloud systems during Phase III of GATE. Part III: Effects of cloud microphysics. *J. Atmos. Sci.,* **56,** 2384–2402.

Harrington, J. Y., 1997: The effects of radiative and microphysical processes on simulated warm and transition season Arctic stratus. Ph.D. dissertation, Atmospheric Science Paper 637, Colorado State University, 289 pp. [Available from Atmospheric Science, Colorado State University, Fort Collins, CO 80521.]

Hill, G. E., 1974: Factors controlling the size and spacing of cumulus clouds as revealed by numerical experiments. *J. Atmos. Sci.,* **31,** 646–673.

Krueger, S. K., 1997: Intercomparison of multi-day simulations of convection during TOGA COARE with several cloud-resolving models. Preprints, *22d Conf. on Hurricanes and Tropical Meteorology*, Fort Collins, CO, Amer. Meteor. Soc., 63–64.

——, and S. M. Lazarus, 1999: Intercomparison of multi-day simulations of convection during TOGA COARE with several cloud-resolving and single-column models. Preprints, *23d Conf. on Hurricanes and Tropical Meteorology*, Dallas, TX, Amer. Meteor. Soc., 643–647.

——, G. T. McLean, and Q. Fu, 1995: Numerical simulation of the stratus-to-cumulus transition in the subtropical marine boundary layer. Part I: Boundary-layer structure. *J. Atmos. Sci.,* **52,** 2839–2850.

LeMone, M. A., E. J. Zipser, and S. B. Trier, 1998: The role of environmental shear and thermodynamic conditions in determining the structure and evolution of mesoscale convective systems during TOGA COARE. *J. Atmos. Sci.,* **55,** 3493–3518.

Lilly, D. K., 1962: On the numerical simulation of buoyant convection. *Tellus,* **14,** 148–172.

Lin, X., and R. H. Johnson, 1996: Heating, moistening, and rainfall over the western Pacific warm pool during TOGA COARE. *J. Atmos. Sci.,* **53,** 3367–3383.

Liu, C., and M. M. Moncrieff, 1998: A numerical study of the diurnal cycle of tropical oceanic convection. *J. Atmos. Sci.,* **55,** 2329–2344.

Louis, J. F., M. Tiedtke, and J. F. Geleyn, 1981: A short history of the PBL parameterizations at ECMWF. *Proc. Workshop on Planetary Boundary Parameterization*, Reading, United Kingdom, ECMWF, 59–79.

Lukas, R., and E. Lindstrom, 1991: The mixed layer of the western equatorial Pacific Ocean. *J. Geophys. Res.,* **96,** 3343–3357.

Madden, R. A., and P. R. Julian, 1971: Detection of a 40–50 day oscillation of the zonal wind in the tropical Pacific. *J. Atmos. Sci.,* **28,** 702–708.

Moncrieff, M. W., S. K. Krueger, D. Gregory, J.-L. Redelsperger, and W.-K. Tao, 1997: GEWEX Cloud System Study (GCSS) working group 4: Precipitating convective cloud systems. *Bull. Amer. Meteor. Soc.,* **78,** 831–845.

Nicholls, M. E., R. H. Johnson, and W. R. Cotton, 1988: Sensitivity of two-dimensional simulations of tropical squall lines to environmental profiles. *J. Atmos. Sci.,* **45,** 3625–3649.

Olsson, P. Q., J. Y. Harrington, G. Feingold, W. R. Cotton, and S. M. Kreindenweis, 1998: Exploratory cloud-resolving simulations of boundary-layer Arctic stratus clouds. Part I: Warm season clouds. *Atmos. Res.,* **47–48,** 573–597.

Pan, D.-M., and D. A. Randall, 1998: A cumulus parametrization with a prognostic closure. *Quart. J. Roy. Meteor. Soc.,* **124,** 949–981.

Pielke, R. A., and Coauthors, 1992: A comprehensive meteorological modeling system—RAMS. *Meteor. Atmos. Phys.,* **49,** 69–91.

Ramanathan, V., and W. Collins, 1991: Thermodynamic regulation of ocean warming by cirrus clouds deduced from observations of the 1987 El Niño. *Nature,* **351,** 27–32.

Shrinivas, M., and M. J. Suarez, 1992: Relaxed Arakawa–Schubert: A parameterization of moist convection for general circulation models. *Mon. Wea. Rev.,* **120,** 978–1002.

Smagorinsky, J., 1963: General circulation experiments with the primitive equations. Part I: The basic experiment. *Mon. Wea. Rev.,* **91,** 99–164.

Su, H., S. S. Chen, and C. S. Bretherton, 1999: Three-dimensional week-long simulations of TOGA COARE convective systems using the MM5 mesoscale model. *J. Atmos. Sci.,* **56,** 2326–2344.

Tao, W.-K., J. Simpson, and S.-T. Soong, 1987: Statistical properties of a cloud ensemble: A numerical study. *J. Atmos. Sci.,* **44,** 3175–3187.

Trier, S. B., W. C. Skamarock, M. A. LeMone, D. B. Parsons, and D. P. Jorgensen, 1996: Structure and evolution of the 22 February 1993 TOGA COARE squall line: Numerical simulations. *J. Atmos. Sci.,* **53,** 2861–2886.

Walko, R. L, W. R. Cotton, J. L. Harrington, and M. P. Meyers, 1995: New RAMS cloud micro-physics parameterization. Part I: The single-moment scheme. *Atmos. Res.,* **38,** 29–62.

Wang, J., and D. A. Randall, 1996: A cumulus parameterization based on the generalized convective available potential energy. *J. Atmos. Sci.,* **53,** 716–727.

Wang, Y., W.-K. Tao, and J. Simpson, 1996: The impact of ocean surface fluxes on a TOGA-COARE convective system. *Mon. Wea. Rev.,* **124,** 2753–2763.

Webster, P. J., 1994: The role of hydrological processes in ocean-atmosphere interactions. *Rev. Geophys.,* **32,** 427–476.

Wu, X., and M. W. Moncrieff, 1999: Effects of sea surface temperature and large-scale dynamics on the thermodynamic equilibrium state and convection over the tropical western Pacific. *J. Geophys. Res.,* **104,** 6093–6100.

——, W. W. Grabowski, and M. W. Moncrieff, 1998: Long-term behavior of cloud systems in TOGA COARE and their interactions with radiative and surface processes. Part I: Two-dimensional modeling study. *J. Atmos. Sci.,* **55,** 2693–2714.

Wyant, M. C., C. S. Bretherton, H. A. Rand, and D. E. Stevens, 1997: Numerical simulations and a conceptual model of the stratocumulus to trade cumulus transition. *J. Atmos. Sci.,* **54,** 168–192.

Xu, K.-M., 1995: Partitioning mass, heat, and moisture budgets of explicitly simulated cumulus ensembles into convective and stratiform components. *J. Atmos. Sci.,* **52,** 551–573.

Yuter, S. E., and R. A. Houze Jr., 1998: The natural variability of precipitating clouds over the western Pacific warm pool. *Quart. J. Roy. Meteor. Soc.,* **124,** 53–99.